Journal Pre-proof

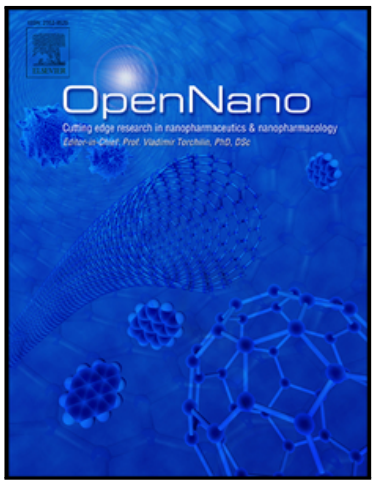

Intra-vaginal Gemcitabine-Hybrid Nanoparticles for effective cervical cancer treatment

Mona Elhabak , Samar Ibrahim , Reem R. Ibrahim

PII: S2352-9520(22)00052-4
DOI: https://doi.org/10.1016/j.onano.2022.100090
Reference: ONANO 100090

To appear in: *OpenNano*

Received date: 19 July 2022
Revised date: 29 September 2022
Accepted date: 30 September 2022

Please cite this article as: Mona Elhabak , Samar Ibrahim , Reem R. Ibrahim , Intra-vaginal Gemcitabine-Hybrid Nanoparticles for effective cervical cancer treatment, *OpenNano* (2022), doi: https://doi.org/10.1016/j.onano.2022.100090

Intra-vaginal Gemcitabine-Hybrid Nanoparticles for effective cervical cancer treatment

Mona Elhabak [a,*], Samar Ibrahim [b], , and Reem R. Ibrahim [a,c].

[a] Department of Pharmaceutics, Faculty of Pharmacy, Ahram Canadian University, Cairo, Egypt.

[b] Department of Pharmacy Practice, Faculty of Pharmacy, Ahram Canadian University, Cairo, Egypt.

[c] Department of Pharmaceutics and Industrial pharmacy, Faculty of Pharmacy, Helwan, Ain Helwan University, Cairo, Egypt.

* Corresponding author .

E-mail address: monaelhabak@hotmail.com

Address: Ahram Canadian university, fourth industrial zone, Cairo, Egypt.

Graphical Abstract

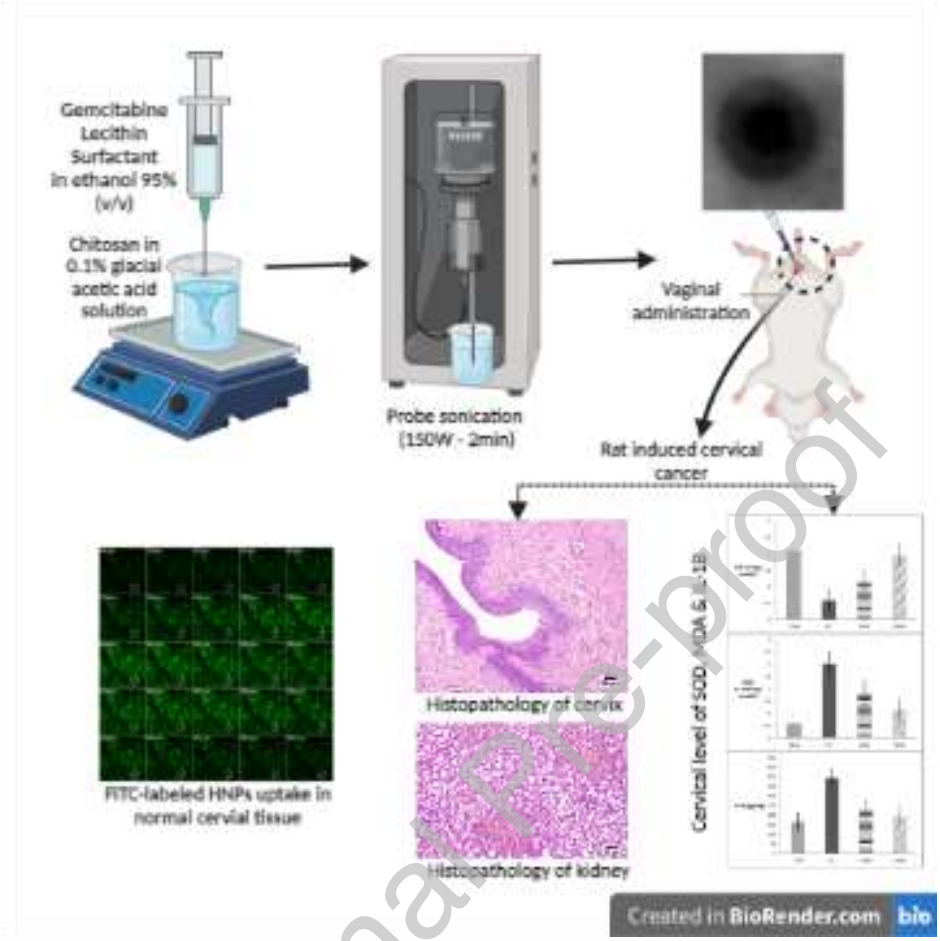

Abstract

Aim: This study aims to develop and evaluate hybrid nanoparticles for the effective intravaginal delivery of the anticancer gemcitabine in cervical cancer rat model.

Methodology: Gemcitabine loaded hybrid nanoparticles (GEM-HNPs) were prepared by ionic gelation method using chitosan, lecithin, and a surfactant. The effect of different variables (chitosan/lecithin ratio, type of lecithin and type/amount of surfactant) were studied on particle size (PS), polydispersity index (PDI), zeta potential (ZP), entrapment efficiency (EE), loading efficiency (% LE). Selected GEM-HNPs were further evaluated for physical morphology using TEM, solid state characterization, percent drug release, in vitro cytotoxicity on Hela cancer cells and in vivo cell uptake using confocal laser scanning microscopy. The efficacy and safety of intravaginal GEM-HNPs in the treatment of cervical cancer were assessed and compared with GEM intravenous administration (IV). Female wistar rats were divided into four groups: Group I: negative control; Group II: positive control (0.2 ml trichloroacetic acid) induced cervical cancer; Group III: rats receiving intravaginal GEM-HNPs and group IV: rats receiving IV GEM. the rat cervices were subjected to histological and biochemical analysis.

Results: The selected GEM-HNPs exhibited acceptable PS of 235.9 ± 11.24 nm, PDI of 0.290 ± 0.004, ZP of 43.8 ± 0.495 mV, high EE of 76.8 ±1.3%, complete drug release in 24 h, enhanced in vivo drug uptake and penetration in cervical cell. The IC50 of pure GEM was found to be insignificantly ($p < 0.05$) different than GEM-HNPs. In-Vivo Antitumor Efficacy and toxicity study on female wistar rat showed that intravaginal administration of GEM-HNPs succeeded to attenuate trichloroacetic acid-induced cervical cancer. This was demonstrated by significant reductions in anti-apoptotic proteins BCl2, P35, angiogenic biomarkers (VEGF, COX2) and inflammatory mediators (IL1b). Additionally, it restored depleted superoxide dismutase (SOD), which in turn reduced MDA levels in cervical tissue. The nephrotoxicity of gemcitabine was reduced compared to the intravenous treatment group.

In conclusion, the current study is the first to demonstrate a successful intravaginal hybrid nanoparticle for the administration of GEM in the treatment of cervical cancer.

Keywords: Gemcitabine, chitosan, Lecithin, Hybrid nanoparticles, Intravaginal, cervical cancer.

1. Introduction

Cervical cancer is considered as the second most prevalent cancer among gynecologic cancers after breast cancer. It is considered one of the main leading cancer related mortalities in women, worldwide [1]. Conventional chemotherapy, administered through intravenous (IV) infusion, may cause many severe systemic toxicities. Hence, there is a great need to develop localized, safe and effective delivery systems against cervical cancer to reduce the toxicity and side effects caused by conventional therapy. The last few years, the vaginal route has gained great attention. The vagina is characterized by its high vascularization, ability to bypass first pass metabolism and to protect drug from enzymatic and acidic degradation, resulting in higher bioavailability and enhanced drug efficacy. The intravaginal route represents an appropriate route for both local and systemic absorption and for better patient compliance [2].

Gemcitabine (GEM) is a deoxycytidine analogue. It was originated as an antiviral drug then it was developed for the treatment of cancer [3]. It is broadly used for the treatment of solid

cancer of pancreas, neck, head, breast, bladder, colon and ovary. GEM is characterized by a short half- life of 8-17 min in human plasma [4]. GEM treatments are afflicted by many problems such as low drug sensitivity, short half-life and dose related toxicities such as hematological, gastrointestinal, hepatic and renal toxicities) [5]. As a result of the short half- life of GEM and its rapid metabolism, continuous IV infusion is required to attain the required therapeutic concentration [6]. Furthermore, the progress of chemo-resistance that occurs in some cancers due to the loss of transporter proteins and kinases needed for phosphorylation represents a big drawback of GEM therapy [7]. Accordingly, an appropriate drug delivery system and alternative route of administration would be developed to overcome these side effects and to achieve the full anticancer potential of GEM. No previous data was reported for intravaginal administration of GEM. Various drug delivery systems as liposomes, polymeric nanoparticles (NPs), metal-organic prodrugs were stated [8]. Nowadays, the use of nanotechnology has been extended to innovate new systems; which can enhance the bioavailability and therapeutic effect of the drugs. Among these systems, the use of lipid polymer hybrid NPs (LP-HNPs) has proved to be a successful one which merges the features of both lipid-based and polymeric nanostructures with avoiding their drawbacks [9]. GEM loaded LP-HNPs with a lipid core and polymeric shell were previously prepared adopting double emulsion solvent evaporation method. Polylactic co glycolic acid (PLGA 50:50), soya phosphatidylcholine and 1,2-distearoyl-sn-glycero3-phosphoethanolamine-N-[methoxy (polyethylene glycol)-2000 (DSPE-PEG2000) with or without cholesterol were utilized for the formulation of LP-HNPs. Although these systems achieved improved GEM half-life and efficacy, they exhibited only around 45% encapsulation efficiency (%EE)[10].

In this study, GEM was prepared in the form of hybrid lipid polymer nanosystem. The natural aminated polysaccharide, biodegradable, biocompatible, and nontoxic polymer, chitosan, was used as a polymeric core with a satisfactory absorption profile [11]. Chitosan has a reactive amine and hydroxyl functional groups, which permits easy preparation of hybrid lipid polymeric nanoparticles through ionic interaction with the negatively charged lipids. Also, chitosan shows mucoadhesive properties to negatively charged biological membranes [12].The natural component of the biological membranes, lecithin was selected as the lipid constituent in our hybrid NPs owing to its superior biocompatibility [13]. Lipid chitosan HNPs have the advantage of combining the structural integrity of polymeric NPs and the biocompatibility of liposomal drug delivery systems

[14]. HNPs can be formed by the interaction between the positive charge of chitosan and the negative charge of lecithin. The incorporation of non- ionic surfactant was adopted to enhance penetration of the lipid polymer hybrid vesicles [15].

Our study focuses on the formulation of intravaginal GEM-loaded lecithin chitosan hybrid nanoparticles (GEM-HNPs), composed of lecithin as lipid core, chitosan as a mucoadhesive polymeric shell and a penetration modifier to maximize drug encapsulation and to promote efficient vaginal cell penetration and uptake. The intravaginal administration of GEM-HNPs aims to maximize the therapeutic efficacy of GEM caused by cervical targeting, as well as to reduce the organ toxicity that may be induced by IV administration.

2. Materials and methods

2.1. Materials

Gemcitabine base (GEM) was purchased from Carbosynth, UK, Chitosan (Low molecular weight, approximately 93 % deacetylated) was purchased from Sigma-Aldrich (USA). Soy lecithin (Lipoid S75) and egg lecithin (Lipoid E80) were obtained from Lipoid AG-Germany) as a gift sample. Labrafac, labrasol and transcutol, as a gift sample, were provided by gattefose, France. Fluorescein isothiocyanate (FITC) dye was purchased from Acros organics, USA. Trichloroacetic acid 99.6% (TCA) was purchased from Thermo-fisher, Germany. Ethanol (95%), glacial acetic acid, sodium acetate, were obtained from El-Nasr pharmaceutical chemicals Co. (Cairo, Egypt).

2.2. Preparation of GEM-loaded Lecithin-chitosan hybrid nanoparticles (GEM-HNPs)

GEM-HNPs were prepared by applying an earlier stated ionic gelation method with some modification [13]. An accurately weighed amount of chitosan was dissolved in 5 mL (0.1 % v/v) acetic acid in water. Lecithin was dissolved in 95% ethanol (2 mL) then GEM and surfactant were added to the same ethanolic solution. The mixture was subjected to ultrasonic vibrations for 5 min in water bath sonicator (Crest Ultrasonics Corp., NJ, USA) till complete dissolution of all used materials. The clear ethanolic solution was then injected slowly by a syringe into the chitosan solution under stirring at 250 rpm for 1h to equilibrate and evaporate the ethanol. The produced blend was then subjected to probe sonication (VCX600, Sonics and Materials, USA), activated for 3 s every 6 s at 150 W for 2 min. The amount of GEM was kept constant (50mg) in all the tried formulations. Different amounts of chitosan (10, 20 and 30mg), Lecithin (100 and 150mg) and

surfactant (0, 50 and 100mg) were assessed for their effects on PS, PDI, ZP, EE and LE. The composition of all the prepared formulations (GEM-HNPs) is presented in Table (1).

2.3. *In vitro* characterization of GEM-HNPs

2.3.1. Determination of Particle size (PS), polydispersity index (PDI), and zeta potential (ZP)

The prepared GEM-HNPs were evaluated for their average PS, PDI, and ZP at 25℃ using Malvern zeta-sizer (Worcestershire, UK). The determinations were conducted in triplicates, and were denoted as average ± standard deviation (SD).

2.3.2. Determination of entrapment efficiency (EE%) and Loading efficiency (LE%) percent

GEM EE% and LE% were calculated directly after the separation of the prepared GEM-HNPs using ultra-cooling centrifuge set at 28,000 rpm and 4ºC (Sigma 3-30 KS, Sigma Laborzentrifugen GmbH, Germany) for 30min. The residual NPs were collected and subjected to disruption using 10 mL of ethanol and glacial acetic acid mixture (1:0. 1 v/v). GEM was then measured by a UV-Vis spectrophotometer at λmax 269 nm (Jasco, V-630). EE% and LE% of GEM-HNPs were done in triplicates and were calculated as follows:

$$EE\% = E / I \times 100 \qquad (1)$$

$$LE\% = E/(E + L + C + S) \times 100 \qquad (2)$$

Where E: the amount of entrapped drug, I: the initial amount of drug, L: the amount of lipid, C: the amount of chitosan and S: the amount of surfactant [16].

2.3.3. Transmission electron microscopy (TEM)

The morphology and shape of the selected GEM-HNPs formulation were examined by TEM (Joel JEM 1230, Tokyo, Japan). NPs dispersion (50 ul) was fixed on a metallic grid, and allowed to completely dry at 25±2℃ for imaging.

2.3.4. Fourier transform-infrared spectroscopy (FT-IR)

To detect any incompatibilities between GEM, and the selected GEM-HNPs, the samples were investigated via an FT-IR spectrophotometer (Shimadzu, IRSpirit, Tokyo, Japan). GEM, egg lecithin, chitosan, transcutol, their physical mixture and the selected GEM-HNPs spectra were scanned from 4500 to 500 cm $^{-1}$ [17].

2.3.5. *In vitro* release study

The release of GEM from the selected GEM-HNPs formulation and the pure drug was carried out in an incubator shaker (Unimax, IKA, Germany) using dialysis bag method [18]. A volume of 1mL of the NPs dispersion equivalent to 10 mg of GEM was put in dialysis bag (MWCO 14Kda, thermo fisher scientific, USA) and dipped in 50 mL acetate buffer (pH 4.5, mimicking vaginal pH) at 37 ± 0.5 °C for 24 h at 50 rpm. Samples (2 mL) were withdrawn at certain times (0.5, 1, 2, 3, 4, 6, 8, 12, and 24 h). The samples were evaluated for the cumulative percentages of GEM released spectrophotometrically at a wavelength of λ_{max} 269 nm and the averages (±SD) were plotted versus time [19]. All measurements were conducted in triplicate.

2.4. *In vitro* cytotoxicity study

Cell viability study was performed on cervical cancerous cells (Hela cells) to evaluate the cytotoxicity of the selected GEM-HNPs. Hela cells were provided by Nawah Scientific Inc., Egypt. Cells were kept in RPMI media containing streptomycin (100mg/mL), penicillin (100 units/mL) and fetal bovine serum (10% v/v) in humidified 5 % (v/v) CO_2 atmosphere at 37º C. Sulforhodamine- B assay (SRB) was used to evaluate cytotoxicity study [20]. A volume of 100 µL cell suspension (5 x 10^3) were seeded in each well of 96-well plates and incubated at 25 ºC. After 24-hour incubation, another aliquot of 100 µL media comprising GEM solution, GEM-HNPs or drug free HNPs at various concentrations (0.01 - 100 µg/mL) were added to the cells. After 48h exposure, a volume of 150 µL of 10 % TCA was added to the cells for fixation then cells were incubated at 4ºC for 1h. Cells were then rinsed five times using purified water. This was followed by the addition of 0.4 % w/v SRB solution (70 µL) and incubation for 10 min at room temperature in dark. Acetic acid (1 %) was used for washing and plates were allowed to dry overnight. Protein-bound SRB stain was dissolved using 150 µL TRIS (10mM). The absorbance was measured by microplate reader (BMG LABTECH®- FLUO star Omega, Germany) at 540 nm.

2.5.*In vivo* study

Animals

Twenty-four female Wistar Albino rats were provided from the holding company for biological Products and vaccines, VACSERA, Egypt. The age of rats was about four months with an average weight of 150–170 g. All experimental procedures followed the Ethical Committee guidelines of Faculty of Pharmacy, Ahram Canadian University (Ceu622). The animals were kept in stainless steel cages at 22±2°C and humidity of 45%-50%. Free access to water *ad libitum* and standard diet were allowed to all animals.

2.5.1. *In vivo* fluorescent imaging using confocal laser scanning microscopy (CLSM)

Confocal laser microscope **(**LSM 710, ZEN 2.3, Carl Zeiss, Germany) was used to evaluate NPs uptake and internalization in cervical tissues. On the day of the experiment, six rats were categorized into two groups (three rats per group). The selected FITC labeled HNPs were formulated with the method employed for the preparation of GEM-HNPs previously described under section (2.2), except that the same dose of the drug (GEM) was replaced with 1mg FITC dye. A specified volume (100uL) of FITC dye solution (1 mg/mL) and the selected dye labeled HNPs (containing 0.1 mg dye) were applied in the vagina of group I and group II, respectively. Two hours after applying the treatment, the rats were ended by decapitation. Then, the cervix was removed and rinsed with normal saline solution. The cervices were cut and fixed, then directly examined by CLSM. For nuclear staining, the tissues were covered with 50 µL 4′,6-diamidino-2-phenylindole (DAPI) (200 µg/mL) prepared in PBS. After 20 min incubation in the dark at room temperature, the samples were washed three times with PBS. Green channel for FITC: excitation at 543 nm and blue channel for DAPI: excitation at 405nm were used. Stacked images (Optical slice sections of approximately 2µm) were analyzed using ZEN 2.3 software (blue edition).

2.5.2. *In-Vivo* Antitumor Efficacy and toxicity

Experimental design

Based on previous experimental research showing the carcinogenicity of trichoroacetic acid (TCA) and its ability to induce tumors in different organs in rodents, TCA was chosen for the induction of cervical cancer in our study [21]. A pilot study (using 10 rats) was conducted to determine the LD100 of intravaginal TCA at doses of 0.1, 0.2 and 0.3 mL. The stage of the estrous

cycle was determined by histological examination of vaginal swabs. Animals were sacrificed after 3 estrous cycles and histopathological examination was performed. The results showed that a single 0.2 ml dose of intravaginal TCA was sufficient to induce cervical cancer.

The animals were categorized into four groups: group I (CON n=6): negative control; group II (PC, n=6): positive control, induced cervical cancer, rats received no treatment; group III (GEM, n=6): 15 days after induction of cervical cancer, rats received 5mg IV GEM (GEMZAR®) twice a week for one month; group IV (GEM-HNPs, n=6): 15 days after induction of cervical cancer, rats received intravaginal 100 µl GEM-HNPs equivalent to 2.5mg GEM twice per day twice a week for one month. Rats were sacrificed after 3 estrous cycles and cervices of the rats were removed for evaluation

2.5.2.1. Enzyme-linked immunosorbent assay (ELISA)

The cervices were weighed and homogenized on ice in fresh lysis buffer (catalog: IS007 (pH 7.2) and protease inhibitor cocktail (Sigma-Aldrich, USA), then incubated at 4 °C for 90 min. Afterwards, they were centrifuged at 10,000 rpm for 5 min. The concentrations of VEGF, Bcl2, Cox2 and IL1B in the supernatant were detected by ELISA following the manufacturer's instructions (Life Span Bio Sciences, USA, cat. no. LS-F40468).

2.5.2.2. Reverse transcription-quantitative polymerase chain reaction (RT-qPCR)

For measuring the mRNA levels, the cervices were removed and frozen under nitrogen. total RNA isolation and DNase treatment were carried out following the manufacturer's instructions (TRIzol® Reagent Cat# R2072, ZYMO RESEARCH CORP. USA). For qPCR, RNA samples were reverse transcribed using Prime Script™ RT Reagent (Cat. No. 12594100, Thermo Fisher Scientific, Waltham, MA, USA). Relative amounts of target mRNA were measured using SYBR® Premix Ex Taq™ II (Takara Bio Inc.) respecting the manufacturer's directions. Temperature cycling conditions: 15 minutes at 94°C, then for 15 seconds (40 cycles), 30 seconds at 60°C and finally 30 seconds at 70°C. The following PCR primers were used: Ki 67, forward GAAAGAGTGGCAACCTGCCTTC and backward GCACCAAGTTTTACTACATCTGCC, GAPDH, forward TGGATTTGACGCATTGGTC and backward TTTGCACTGGTACGTGTTGGAT. The PCR data represents Ct values of assessed gene (ki 67)

versus the corresponding housekeeping gene (GAPDH). Control sample were used to measure the gene expression. Each target gene RQ was quantified and normalized to housekeeping gene based on the calculation of delta-delta Ct (ΔΔCt) by taking 2-ΔΔCt [22].

2.5.2.3. Immunohistochemistry

The expression of P53 protein in cervical tissue samples was performed using immunohistochemical staining. The avidin-biotin complex (ABC) method (Vectastain Elite ABC kit; Vector Laboratories, USA) was adopted for the P53 primary antibody (Santa Cruz Biotechnology, Inc., USA). Samples were heated at 95-100°C in citrate buffer (pH 6.0) to recover antigen then treated with normal horse or goat serum (1.5%) for 30 min. Samples were incubated overnight at 4°C with mouse primary polyclonal antibody (1:100), followed by diluted biotinylated rabbit anti-mouse secondary antibody, then with ABC reagent for 30 min and finally with hydrogen peroxide (0.015%) and diaminobenzidine (0.05%) for 5-10 min. Nucleus staining was done with hematoxylin and P53 was measured.

2.5.2.4. Histological Analysis

Cervices and kidneys tissue were fixed using 4% neutral buffered formalin, handled into paraffin, segmented into 4 µm, and stained by hematoxylin and eosin (H&E). The samples were examined by an optical microscope [23].

2.5.2.5. Cervical antioxidant capacity

To further investigate the regulatory effect of GEM-HNPs treatment on tissue damage and oxidative stress, superoxide dismutase (SOD) levels were measured by measuring superoxide-driven NADH oxidation [24]. Thiobarbituric acid was measured [25] using spectrophotometry at 535 nm.

2.6. Statistical analysis

Statistical analysis was performed using Graphpad Instat. All data obtained were shown as mean ± SD and analysis was carried out using one-way ANOVA followed by Tukey-Kramer multiple comparison post hoc test. $P<0.05$ was used as cutoff value statistical significance.

3. Results and discussion

3.1. Particle size (PS), polydispersity index (PDI) and ZP

The GEM-HNPs were prepared by single step ionic gelation method. The effect of formulation variables on PS, PDI and ZP is shown in table 2. Two types of lecithin (soy and egg) were tried. NPs prepared with soybean lecithin showed significant increase ($p<0.05$) in PS and PDI when compared to egg lecithin containing NPs. Similar results were reported by Fang *etal* who showed that the liposomes formulated with soybean lecithin possessed larger vesicle size than that of egg yolk lecithin prepared liposomes when the type of sterol was kept constant. The increase in size may be attributed to the higher phosphatidylcholine content in soybean lecithin than that in egg **yol**k lecithin [26].

It is obvious in table 2 that decreasing lecithin/chitosan ratio from 10:1 to 3:1 was accompanied with significant increase ($p<0.05$) in PS from 155.2 ± 0.424 (F4) to 184.6 ± 5.23 (F5). Similar results were reported by [27], who observed an increase in particle diameter with increasing chitosan content in HNPs. This might be attributed to the increase in the viscosity of the resultant dispersion which led to a decrease in the evaporation rate of the organic solvent, and consequently a larger PS. Also, the increased viscosity at higher polymer concentration presented a resistance to the breakdown of the droplets into smaller particles and decreased the effect of shear force produced by the stirring [28]. PS significantly ($p\leq0.05$) increased with the incorporation of labrafac, labrasol and transcutol (50mg) as penetration enhancer in the formulations (F6, F7 and F8). Increasing transcutol amount up to 100mg (F9) resulted in a significant decrease ($p\leq0.05$) in PS as shown in table 2. The presence of penetration enhancer increased PS of the prepared nanoparticles. This is attributed to the fact that penetration enhancer is able to intercalate into the phospholipid bilayer leading to particle swelling with liquid oil [29]. Further increase in transcutol amount was able to solubilize the lecithin bilayers which led to a decrease in PS [30]. The increase in the amount of liquid oil caused a decrease in the viscosity and surface tension and hence smaller PS was obtained. Similar results were reported during the formulation of nanostructured lipid carriers loaded with fenofibrate [29].

The PDI of the prepared GEM-HNPs (F2 to F5) were around 0.3 indicating acceptable particle uniformity. Phospholipids based nanovesicles with PDI ≤ 0.3 are considered to be acceptable and

designates homogenous particle distribution [31]. No significant change was observed in PDI of the prepared HNPs F2 to F5 denoting that varying lecithin to chitosan ratio from 10:1 to 3:1 had no effect on particle uniformity.

ZP is an essential parameter for the estimation of NPs stability. Zeta potential ≥ ±30 mV indicates adequate stability [32]. Egg yolk lecithin NPs with ZP value of 41.7 ± 0.849 mV were the most stable. While soy bean lecithin NPs exhibited significantly lower ZP (14.8 ± 2.05) indicating poor stability. Soy lecithin contains negatively charged phosphatidylinositol while egg lecithin is composed of mainly phosphatidylcholine [33]. This might be the reason for the lower ZP of the HNPs prepared with soy lecithin and hence their poor stability.

NPs prepared with egg lecithin/chitosan ratio 10:1, 7.5:1 and 5:1 (F4, F3 and F2 respectively) revealed insignificant change in ZP. Increasing chitosan content in F5 produced a significant increase in ZP as shown in table 2. All the prepared HNPs (F2 to F5) were characterized by large positive ZP confirming their stability for long shelf life. This positive charge returns to the positively charged chitosan. Previous studies demonstrated that the PS and ZP of HNPs were dependent on lecithin/chitosan ratio. Ratios from 5:1 to 20:1, resulted in positively charged particles with ZP around 40mV, PS < 280nm and PDI < 0.2. Increasing lecithin/chitosan ratio from 30:1 to 50:1 led to large increase in PS, aggregation and sedimentation. Further increase in the ratios from 60:1 to 80:1, surface charge inversion from positive to negative was obtained and particles with negative charge (−42 mV), PS (400 nm) and PDI (≥0.231) were produced [34]. As shown in table 2. The presence of penetration enhancers (labrasol and transcutol) in F7 and F8 did not alter the surface charge of the HNPs and with increasing the concentration of transcutol as in F9, ZP values remained unchanged. Similar results were reported by [30], where the ZP values were invariable with the presence and varying the concentration of transcutol in diclofenac loaded and free liposomes prepared with soy lecithin.

3.2. Encapsulation Efficiency (EE%) and Loading Efficiency (LE%)

Results of EE% and LE% of the different formulations were shown in table 2. The GEM-HNPs showed an increased encapsulation of gemcitabine, due to the lecithin layer. This lecithin layer caused better solubility of the drug in the lipophilic phase and incorporation inside the hybrid system. This resulted in an increased EE %, as it prevented leakage of the encapsulated GEM [13].

We can observe from table 2 that GEM-HNPs prepared with egg lecithin resulted in significantly higher EE% when compared to soy lecithin prepared HNPs. This was in contrary to previous study where encapsulation of caffeine was insignificant when both types of lecithin were tried for the preparation of caffeine loaded liposomes [35]. As shown in table 2, decreasing chitosan/lecithin ratio in F2-F4 had no significant effect ($P>0.05$) on GEM EE% (around 55%w/w). Further increase in chitosan amount (F5) led to significant increase ($P<0.05$) in EE% to 68.5 ±2.1 % w/w. The increment in EE % indicated a stable interaction between the negative charges in the lipid and the positive charges of chitosan and hence balanced conjugate was obtained [36]. The addition of labrafac lipophile in F6 as penetration enhancer had insignificant effect on EE% ($P>0.05$). On the other side, labrasol (F7) showed significant decrease ($P<0.05$) in EE% to 37 ±4.6% w/w when compared to penetration enhancer free formulation (F5). The addition of transcutol in F8 resulted in a significant increase ($P<0.05$) in EE% to 76.8 ±1.3% w/w. While doubling the amount of transcutol in F9 lead to significant decrease ($P<0.05$) in EE% to 54.7 ±2.5%w/w. This might be attributed to that the increase in transcutol amount in formulation F9 decreased PS and hence EEn%. Also, the decrease in viscosity provoked by the penetration enhancer may cause the diffusion of the drug throughout the nanovesicles assembly leading to a decrease in EE% [28]. The three used penetration enhancers revealed different effect on drug entrapment. This could be explained by the difference in solubility of gemcitabine in each type [37]. The effect of these three penetration enhancers on the EE % of the acetazolamide in penetration enhancing hybridized vesicles was previously studied by Hathout RM et al 2015. They had positive effect on EE % as arranged in the following order: transcutol > labrafac lipophile > labrasol [15].

Formulation F8 prepared using 50mg GEM, 100mg egg lecithin, 30mg chitosan and 50mg transutol and showing maximum EE% and acceptable PS, PDI and ZP was selected for further characterization and in vivo study.

3.3. Morphology by Transmission Electron Microscopy

The morphology of Gem-HNPs (F8) was visualized by TEM. NPs appeared as spheres with dark hydrophilic polymeric core surrounded by a lighter hydrophobic shell. The hydrophilic phosphotungistic acid dye concentrated in the aqueous core is responsible for its darker color (Fig. 1) [38]. The gray dots and background represent the dispersion medium stained with

phosphotungistic acid dye. [39]. PS measured by TEM was around 140nm (Fig 1). The average hydrodynamic diameter measured by dynamic light scattering (DLS) technique was larger than the size recorded by TEM [38]. The difference in size obtained by DLS and TEM is mainly due to nanoparticles shrinkage during the drying stage in the sample preparation. DLS is more reliable for PS measurement as the image taken by TEM could be away from the mean PS and hence a minimum of hundred TEM photos will be required [15].

3.4. FTIR

The FTIR spectra of GEM, lecithin, chitosan, transcutol, the physical mixture, and GEM-HNPs (F8) are presented in Fig. 2. The IR spectrum of GEM (Fig. 2a) displayed definite peaks at 3444, 1649, 1521, 1053, and 779 cm^{-1} that belonged to the existence of amine N–H stretching, amine bending vibration, C=C aromatic, C–N amines, and C–H aromatic, respectively [40]. FTIR spectrum of egg lecithin (Fig. 2c) showed characteristic bands at 2922, 1732, 1467, 1247 and 1064 cm^{-1} and 2921 cm^{-1}corresponding to -CH stretching, C=O stretching, C-H bending vibration, P-O and P-O-C stretching vibration respectively [41]. FTIR spectrum of chitosan (Fig. 2b) revealed peaks at 3362, 1646 and 1418 **c**m^{-1} of N-H and OH stretching, N-H bending and C-H bending respectively. All the peaks are present in the physical mixture and GEM-HNPs. Transcutol FTIR spectra (Fig. 2d) showed characteristic bands at ~3600, 2871 and at 1110 and1067 cm^{-1} correlating to O-H, C-H and C-O stretching [41]. In the spectrum of GEM-HNPs (Fig. 2f), the intensity of characteristic peak of GEM at 1649 cm^{-1} was reduced confirming the incorporation of GEM into NPs. In both the physical mixture and GEM-HNPs spectra (Fig. 2e & f), a shift in the N-H stretching peak of chitosan and P-o stretching peak of lecithin were observed. The interaction between the negatively charged lecithin and the positively charged chitosan might be responsible for this shift. Similar results were reported by [42].

3.5. *In vitro* release study

The release profiles of GEM-HNPs and pure GEM powder are displayed in Fig 3. GEM-HNPs displayed a bi-phasic release pattern with an initial drug burst of ~70% in the first 2h, followed by sustained drug release up to 24h. The existence of the drug in the outer layer along with the incorporation of high amount of transcutol in the formulation were responsible for the initial burst and acceleration of drug release. GEM deep in the NPs core was slowly released by diffusion or

polymer erosion mechanism [29]. On the other hand, GEM powder showed complete dissolution within 1h.

3.6. *In vitro* cytotoxicity study

The therapeutic efficacy and cytotoxicity of the prepared HNPs were assessed against HeLa cells by SRB assay. GEM and GEM-HNPs groups inhibited cell growth in a dose-dependent manner (Fig. 4). The IC_{50} was determined based on Boltzman sigmoidal concentration/response curve equation using the nonlinear regression models (Graph Pad, Prism version 5). *In vitro* outcomes revealed insignificant differences between GEM and GEM-HNPs groups with IC50 of 0.07 and 0.08ug/mL respectively. GEM base is a small lipophilic molecule able to cross plasma membrane into cells by simple diffusion due to its solubility in the hydrophobic region of the phospholipid bilayer [43]. The positive charge of chitosan in GEM-HNPs in addition to the fusion of phospholipids with cell membrane allowed efficient cell attachment and cellular uptake [44] [45]. The non-difference in cytotoxicity might be due to the absence of enhanced permeation retention (EPR) effect *in vitro* and both formulations were applied directly onto the cells [46]. The superiority of the HNPs would be emphasized *in vivo* study.

3.7. *In vivo* study

3.7.1. *In vivo* fluorescent imaging using CLSM

The confocal microscopic images showed the difference in uptake of the dye labelled HNPs and the dye solution inside the cervical tissues. The intensity of the green fluorescence in Fig 5(a) was prominent in FITC labelled NPs treated cervical tissue suggesting increased NPs uptake. However, FITC solution treated cervices showed no remarkable fluorescence in Fig 5(b). The z-slices (Fig. 5c) showed that FITC labelled NPs were present in different planes throughout the thickness of the cervical tissue. Cross-sectional slices confirmed that NPs were indeed inside the tissues. The mucoadhesive property of chitosan helped in extending drug residence time on the mucosal tissue. Moreover, the interaction between positive charges on the HNPs surface with the negatively charged mucosal membrane along with the fusion of lecithin with cell membrane promoted dye penetration and *in vivo* uptake [45].

3.7.2. Assessment of angiogenic biomarkers, Lipid peroxidation, antioxidant and anti-inflammatory activity

Fig. 6(a) and (b) show the relative expression levels of VEGF and COX-2 in cervical tissue, respectively. The relative expression levels of VEGF and COX-2 in the cancer group (PC) rats were significantly high compared to the CON group ($P<0.001$). Intravenous administration of GEM and intravaginal GEM-HNPs significantly blocked the increase of VEGF by 1.72% compared with the disease control group. In contrast, Cox2 decreased by 2.03% and 1.46%, and Cox2 decreased by 2.03% and 3.51%, respectively. A significantly significant reduction in VEGF and COX2 was observed in rats treated with GEM-HNP compared to GEM treatment ($p<0.001$). Administration of TCA resulted in a significant decrease of 3.64% in total cervical SOD activity (Fig. 7a), but increased MDA (Fig. 7b) and IL1B levels (Fig. 7c) by 4%, 0.93% and 2.36% compared to normal values in control rats Compare. These dearrangement were effectively attenuated in rats treated with IV GEM or intravaginal GEM-HNP. It was found that compared with disease model rats, GEM-HNPs significantly increased cervical SOD content by 3.38%, but significantly decreased MDA tissue content and IL1B content by 3.51% and 2.01%, respectively. Furthermore, GEM-HNPs had a significant effect ($P<0.001$) on the above markers compared with iv administration. Greenhough et al previously reported that the increased expression of COX-2 inhibited apoptosis, suppressed immunity, promoted angiogenesis, and enhanced the invasion of malignant cells [47]. Moreover, COX-2 inhibitors role in cervical cancer was reported by Wang *etal* [48]. In the present study, IL1B was overexpressed in cervical cancer. Similarly, COX-2 overexpression in disease control group provided strong evidence for their role in tumor-induced angiogenesis in cervical cancer. COX-2 has an indirect pathway on tumor angiogenesis mediated by overexpression of angiogenic factors such as VEGF. This pathway induces the synthesis of prostanoids, that stimulates proangiogenic factors expression [49]. This revealed that both COX-2 and VEGF were critical for tumor angiogenesis in cervical cancer.

Furthermore, the present study revealed that VEGF strong expression was found in rats bearing cancer. VEGF, vascular growth factor that regulate endothelial cells proliferation, migration and angiogenesis, with high specificity [50]. GEM-HNPs was able to decrease the expressions of IL1B, Cox2 and VEGF protein in tumor tissue.

The Increase in oxidative stress caused an imbalance between free radical production and cellular defence mechanisms. This played an important role in cancer as well as cancer treatment

side effects [51]. SOD is a major antioxidant enzyme widely distributed in all cells. SOD protects cells from lipid peroxidation and catalyses the disproportionation of superoxide anion to oxygen and hydrogen peroxide [52]. Cervical inflammation increases SOD production, which in turn increases intracellular hydrogen peroxide, creating an environment conducive to DNA damage and cancer development and progression [53]. MDA is a highly cytotoxic end product of lipid peroxidation and acts as a tumor promoter [54]. Previous research also showed that MDA levels were significantly elevated in the blood of patients with different types of cancer compared to healthy controls [55]. Therefore, oxidative stress has been recognized as a major factor in the early stages of carcinogenesis.

3.7.3. Cervix histopathology

Microscopic examination of control group revealed normal exocervical mucosa histology with intact propria-submucosa of thick irregular connective tissue. The tunica muscularis is formed of outer longitudinal and inner circular smooth muscle layers (Fig. 8a). The mucosal surface of the PC group showed papillary projection of the mucosal epithelium into the lumen of the cervix. The mucosa showed hyperplastic stratified epithelium with round nuclei, hyperchromasia and dysplastic changes in some circumstances. Hyperplasia of goblet cells were detected in some examined sections associated with vacuolation of the hyperplasic epithelial cells. Mild anisocytosis and anisokaryosis were observed (Fig. 8b). Administration of GEM via IV route showed moderate improvement in the cervical mucosa. Moderate hyperplasic stratified mucosal surface associated dysplastic changes characterized by excessive vacuolated epithelial cells was observed. Fewer number of neutrophilic infiltrations was also detected in the mucosal surface (Fig. 8c). Marked improvement was noted in GEM-HNPs group. Several examined sections revealed mild hyperplasia in the stratified mucosal epithelial layer. Apparently normal cervical mucosa was detected in some examined sections (Fig. 8d). The reversal of the histopathological damage in the cervix tissue might be caused by the reduced or complete inhibition of the oxidative stress accompanied by an improvement in the antioxidant status.

3.7.4. Assessment of apoptosis-related proteins in tumor tissue

As illustrated in Figure 9, the level of anti-apoptotic protein Bcl-2 in the disease control group was significantly increased by 3.12% when compared to CON group ($P < 0.001$). IV GEM

significantly reduced BCL-2 expression by 1.52% when compared to PC group ($P < 0.001$). In addition, compared with the PC group, the Bcl-2 level in the cervical tissue of the GEM-HNPs group was significantly decreased by 2.27%, which was significantly lower than the IV GEM treatment group ($P<0.001$). To further investigate the mechanism of GEM-HNPs-mediated apoptosis in tumor tissues, the expression of P53 protein was measured by immunohistochemical assay. As shown in Fig. 10, CON group showed no to weak p53 expression in the cervical mucosa and submucosa (Fig. 10a). Meanwhile, strong p53 expression was found in the cervix of the PC group (Fig. 10b), moderate to low expression was found in the IV GEM group (Fig. 10c), and low to weak levels were found in the PC group of p53 expression. Cervical layer of the intravaginal GEM-HNP-treated group (Fig. 10d). Apoptosis, as a homeostatic mechanism, which balances cell death and cell division, preserves a proper cell number in tissues [56]. Bcl-2, a specific gene, plays an important role in apoptosis regulation [57]. It resists cell death and prolongs its lifespan [58]. p53, a transcription factor, engaged in cell cycle control, cell differentiation, apoptosis, gene regulation, and tumor suppression (Olivier [59]. In conclusion, our study establishes a paradigm in which apoptosis is a key component of p53-mediated tumor suppression.

3.7.5. Determination of Ki 67

Real-time PCR showed that (fig. 11) there was a statistically significant 3.68-fold increase in Ki 67 in the PC group compared to the CON rats ($p<0.001$). However, both IV GEM and intravaginal GEM-HNP showed a statistically significant 1.39- and 2.09-fold downregulation of Ki 67, respectively ($p<0.001$). A significant decrease in Ki67 was observed with GEM-HNPs treatment compared to IV GEM ($p<0.001$). Ki-67 is used as a biomarker of cervical lesions and a diagnostic factor for tumor growth, proliferation and prognosis [60]. In this study, increased Ki-67 in the positive control group identified cervical cancer lesions that were reversed by GEM-HNPs, suggesting a favourable effect in suppressing cancer lesions.

3.7.6. Assessment of toxicological effects of GEM-HNPs treatment in tumor bearing rats

The histological alterations in kidney tissues are shown in Figure 12. Microscopic examination of kidneys tissue from the negative control group (Fig. 12a) revealed the normal histology of both renal cortex and medulla. Regarding PC group, Necrobiotic changes were detected in several examined sections associated with variable number of inflammatory cells

infiltration. Congested interstitial blood vessels were commonly observed in the affected renal parenchyma especially in the medullary region. Fewer mineralized foci were noticed in the necrotic renal tubules (Fig. 12b). Examination of IV GEM group showed severe diffuse tubular necrosis that was characterized by necrotic epithelial lining renal tubules with eosinophilic debris and pyknotic nuclei in the renal cortex and medulla. Congested interstitial blood vessels were also observed in the renal parenchyma accompanied by congested glomerular capillary tufts. Interstitial nephritis was detected in several sections associated with mineralization of necrotic renal tubules (Fig. 12c). Intravaginal GEM-HNPs group showed less histopathological alterations compared to PC and IV GEM group. Fewer necrobiotic changes were observed scattered in cortex and medulla. Multifocal interstitial nephritis was noticed in sporadic cases (Fig. 12d). The perfect chemotherapy drug not only has the benefit of inhibiting the growth of tumor cells, but also has minimal toxicity to normal tissues [61]. Kidney susceptibility to various potentially nephrotoxic drugs can be attributed to multiple functional properties of the kidney, including an abundant blood supply that ensures high clearance of toxins [62]. The current study suggests that intravaginal administration of GEM may prevent systemic nephrotoxicity.

4. Conclusion

GEM-HNPs were successfully prepared with chitosan/lecithin ratio 1:3 and transcutol (50mg) as surfactant using ionic gelation method. GEM-HNPs showed PS :235.9 ± 11.24, PDI: 0.290 ± 0.004, ZP: 43.8 ± 0.495. GEM was efficiently encapsulated in the hybrid NPs (EE%: 76.8 ±1.3). They also conferred in vivo deep penetration through the vaginal mucosa and effective uptake in cervical cell as visualized by CLSM. Intravaginal GEM-HNPs administration in cervical cancer induced female Wistar Albino rats significantly reversed TCA-induced histopathological and biochemical changes. It also counteracts GEM nephrotoxicity compared to the IV route. The proposed hybrid nanocarrier system appears to be promising for effective vaginal delivery for safe and effective cervical cancer treatment.

Funding: This research did not receive any specific grant from funding agencies in the public, commercial, or not for profit sectors.

References

1. Shafabakhsh, R., et al., *Resveratrol and Cervical Cancer: A New Therapeutic Option?* Mini Reviews in Medicinal Chemistry, 2022.

2. Oshiro-Júnior, J.A., et al., *Nanoparticle Synthesis and Administration Routes for Antiviral Uses*, in *Viral and Antiviral Nanomaterials*. 2022, CRC Press. p. 77-100.

3. Loo, Y.S., et al., *Recent advances in the development of multifunctional lipid-based nanoparticles for Co-Delivery, combination treatment strategies, and theranostics in breast and lung cancer.* Journal of Drug Delivery Science and Technology, 2022: p. 103300.

4. Saini, K., R. Prabhuraj, and R. Bandyopadhyaya, *Development of mesoporous silica nanoparticles of tunable pore diameter for superior gemcitabine drug delivery in pancreatic cancer cells.* Journal of Nanoscience and Nanotechnology, 2020. **20**(5): p. 3084-3096.

5. Paroha, S., et al., *Recent advances and prospects in gemcitabine drug delivery systems.* International Journal of Pharmaceutics, 2021. **592**: p. 120043.

6. Dubey, R.D., et al., *Recent advances in drug delivery strategies for improved therapeutic efficacy of gemcitabine.* European Journal of Pharmaceutical Sciences, 2016. **93**: p. 147-162.

7. de Sousa Cavalcante, L. and G. Monteiro, *Gemcitabine: metabolism and molecular mechanisms of action, sensitivity and chemoresistance in pancreatic cancer*. European journal of pharmacology, 2014. **741**: p. 8-16.

8. Derakhshandeh, K. and S. Fathi, *Role of chitosan nanoparticles in the oral absorption of Gemcitabine.* International journal of pharmaceutics, 2012. **437**(1-2): p. 172-177.

9. Date, T., et al., *Lipid-polymer hybrid nanocarriers for delivering cancer therapeutics.* Journal of controlled release, 2018. **271**: p. 60-73.

10. Yalcin, T.E., S. Ilbasmis-Tamer, and S. Takka, *Development and characterization of gemcitabine hydrochloride loaded lipid polymer hybrid nanoparticles (LPHNs) using central composite design.* International Journal of Pharmaceutics, 2018. **548**(1): p. 255-262.

11. Thakur, K., et al., *Chitosan-tailored lipidic nanoconstructs of Fusidic acid as promising vehicle for wound infections: An explorative study.* International journal of biological macromolecules, 2018. **115**: p. 1012-1025.

12. Hussein, M.A.M., et al., *Exploring the physicochemical and antimicrobial properties of gold-chitosan hybrid nanoparticles composed of varying chitosan amounts.* International Journal of Biological Macromolecules, 2020. **162**: p. 1760-1769.

13. Khan, M.M., et al., *Lipid-chitosan hybrid nanoparticles for controlled delivery of cisplatin.* Drug delivery, 2019. **26**(1): p. 765-772.

14. Yuan, Y., et al., *Fabrication of psoralen-loaded lipid-polymer hybrid nanoparticles and their reversal effect on drug resistance of cancer cells.* Oncology Reports, 2018. **40**(2): p. 1055-1063.

15. Naguib, S.S., R.M. Hathout, and S. Mansour, *Optimizing novel penetration enhancing hybridized vesicles for augmenting the in-vivo effect of an anti-glaucoma drug.* Drug delivery, 2017. **24**(1): p. 99-108.

16. Affram, K.O., et al., *Cytotoxic effects of gemcitabine-loaded solid lipid nanoparticles in pancreatic cancer cells.* Journal of drug delivery science and technology, 2020. **55**: p. 101374.

17. Nair, A.B., et al., *Development of asialoglycoprotein receptor-targeted nanoparticles for selective delivery of gemcitabine to hepatocellular carcinoma.* Molecules, 2019. **24**(24): p. 4566.

18. Khan, M.M., et al., *Co-delivery of curcumin and cisplatin to enhance cytotoxicity of cisplatin using lipid-chitosan hybrid nanoparticles.* International Journal of Nanomedicine, 2020. **15**: p. 2207.

19. Mohamad Saimi, N.I., et al., *Aerosolized niosome formulation containing gemcitabine and cisplatin for lung cancer treatment: Optimization, characterization and in vitro evaluation.* Pharmaceutics, 2021. **13**(1): p. 59.

20. Koraneekit, A., et al., *Synergistic effects of cisplatin-caffeic acid induces apoptosis in human cervical cancer cells via the mitochondrial pathways.* Oncology Letters, 2018. **15**(5): p. 7397-7402.

21. Purdue, M.P., *Trichloroethylene and cancer*. 2013, Oxford University Press US. p. 844-846.

22. Livak, K.J. and T.D. Schmittgen, *Analysis of relative gene expression data using real-time quantitative PCR and the 2− ΔΔCT method.* methods, 2001. **25**(4): p. 402-408.

23. KINGSBURG, B.J., *HISTOLOGICAL TECHNIQUE: AGUIDE FOR USE IN A LABORATORY COURSE IN HISTOLOGY/BF KINGSBURG AND OA JOHANNSEN*.

24. Beyer Jr, W.F. and I. Fridovich, *Assaying for superoxide dismutase activity: some large consequences of minor changes in conditions.* Analytical biochemistry, 1987. **161**(2): p. 559-566.

25. Ohkawa, H., N. Ohishi, and K. Yagi, *Assay for lipid peroxides in animal tissues by thiobarbituric acid reaction.* Analytical biochemistry, 1979. **95**(2): p. 351-358.

26. Tai, K., et al., *The effect of sterol derivatives on properties of soybean and egg yolk lecithin liposomes: Stability, structure and membrane characteristics.* Food Research International, 2018. **109**: p. 24-34.

27. Hafner, A., et al., *Lecithin/chitosan nanoparticles for transdermal delivery of melatonin.* Journal of microencapsulation, 2011. **28**(8): p. 807-815.

28. Tahir, N., et al., *Development and optimization of methotrexate-loaded lipid-polymer hybrid nanoparticles for controlled drug delivery applications.* International journal of pharmaceutics, 2017. **533**(1): p. 156-168.

29. Tran, T.H., et al., *Preparation and characterization of fenofibrate-loaded nanostructured lipid carriers for oral bioavailability enhancement.* AAPS pharmscitech, 2014. **15**(6): p. 1509-1515.

30. Manconi, M., et al., *Development and characterization of liposomes containing glycols as carriers for diclofenac.* Colloids and Surfaces A: Physicochemical and Engineering Aspects, 2009. **342**(1-3): p. 53-58.

31. Danaei, M., et al., *Impact of particle size and polydispersity index on the clinical applications of lipidic nanocarrier systems.* Pharmaceutics, 2018. **10**(2): p. 57.

32. Wagner, A., K. Vorauer-Uhl, and H. Katinger, *Liposomes produced in a pilot scale: production, purification and efficiency aspects.* European journal of pharmaceutics and biopharmaceutics, 2002. **54**(2): p. 213-219.

33. Palacios, L.E. and T. Wang, *Egg-yolk lipid fractionation and lecithin characterization.* Journal of the American Oil Chemists' Society, 2005. **82**(8): p. 571-578.

34. Sonvico, F., et al., *Formation of self-organized nanoparticles by lecithin/chitosan ionic interaction.* International journal of pharmaceutics, 2006. **324**(1): p. 67-73.

35. Budai, L., et al., *Liposomes for topical use: A physico-chemical comparison of vesicles prepared from egg or soy lecithin.* Scientia pharmaceutica, 2013. **81**(4): p. 1151-1166.

36. Khan, M.M., et al., *Folate targeted lipid chitosan hybrid nanoparticles for enhanced anti-tumor efficacy*. Nanomedicine: Nanotechnology, Biology and Medicine, 2020. **28**: p. 102228.

37. Urimi, D., et al., *Formulation development and upscaling of lipid nanocapsules as a drug delivery system for a novel cyclic GMP analogue intended for retinal drug delivery.* International Journal of Pharmaceutics, 2021. **602**: p. 120640.

38. Zhao, X., et al., *Co-delivery of HIF1α siRNA and gemcitabine via biocompatible lipid-polymer hybrid nanoparticles for effective treatment of pancreatic cancer*. Biomaterials, 2015. **46**: p. 13-25.

39. Elkomy, M.H., et al., *Topical ketoprofen nanogel: artificial neural network optimization, clustered bootstrap validation, and in vivo activity evaluation based on longitudinal dose response modeling.* Drug delivery, 2016. **23**(9): p. 3294-3306.

40. Khare, V., et al., *Synthesis and characterization of TPGS–gemcitabine prodrug micelles for pancreatic cancer therapy.* Rsc Advances, 2016. **6**(65): p. 60126-60137.

41. Perez-Ruiz, A.G., et al., *Lecithin–chitosan–TPGS nanoparticles as nanocarriers of (−)-epicatechin enhanced its anticancer activity in breast cancer cells.* RSC advances, 2018. **8**(61): p. 34773-34782.

42. Murthy, A., et al., *Self-assembled lecithin-chitosan nanoparticles improve the oral bioavailability and alter the pharmacokinetics of raloxifene.* International Journal of Pharmaceutics, 2020. **588**: p. 119731.

43. Zhang, R., et al., *Improving cellular uptake of therapeutic entities through interaction with components of cell membrane.* Drug Delivery, 2019. **26**(1): p. 328-342.

44. Aibani, N., et al., *Chitosan Nanoparticles at the Biological Interface: Implications for Drug Delivery.* Pharmaceutics, 2021. **13**(10): p. 1686.

45. Ma, Q., et al., *Self-Assembled chitosan/phospholipid nanoparticles: from fundamentals to preparation for advanced drug delivery*. Drug Delivery, 2020. **27**(1): p. 200-215.

46. Yu, X., et al., *An in vitro and in vivo study of gemcitabine-loaded albumin nanoparticles in a pancreatic cancer cell line.* International journal of nanomedicine, 2015. **10**: p. 6825.

47. Greenhough, A., et al., *The COX-2/PGE 2 pathway: key roles in the hallmarks of cancer and adaptation to the tumour microenvironment.* Carcinogenesis, 2009. **30**(3): p. 377-386.

48. Wang, Y. and S. Zhang, *Berberine suppresses growth and metastasis of endometrial cancer cells via miR-101/COX-2.* Biomedicine & Pharmacotherapy, 2018. **103**: p. 1287-1293.

49. Chell, S., et al., *Mediators of PGE2 synthesis and signalling downstream of COX-2 represent potential targets for the prevention/treatment of colorectal cancer.* Biochimica et Biophysica Acta (BBA)-Reviews on Cancer, 2006. **1766**(1): p. 104-119.

50. Xiao, X., J. Liu, and M. Sheng, *Synergistic effect of estrogen and VEGF on the proliferation of hemangioma vascular endothelial cells.* Journal of pediatric surgery, 2004. **39**(7): p. 1107-1110.

51. Asadi-Samani, M., et al., *Antioxidants as a double-edged sword in the treatment of cancer*, in *Antioxidants*. 2019, IntechOpen.

52. Valko, M., et al., *Role of oxygen radicals in DNA damage and cancer incidence.* Molecular and cellular biochemistry, 2004. **266**(1): p. 37-56.

53. Willcox, J.K., S.L. Ash, and G.L. Catignani, *Antioxidants and prevention of chronic disease.* Critical reviews in food science and nutrition, 2004. **44**(4): p. 275-295.

54. Zahra, K., et al., *A study of oxidative stress in cervical cancer-an institutional study.* Biochemistry and Biophysics Reports, 2021. **25**: p. 100881.

55. Lepara, Z., et al., *Serum malondialdehyde (MDA) level as a potential biomarker of cancer progression for patients with bladder cancer.* Rom. J. Intern. Med, 2020. **58**(3): p. 146-152.

56. Arur, S., et al., *Annexin I is an endogenous ligand that mediates apoptotic cell engulfment.* Developmental cell, 2003. **4**(4): p. 587-598.

57. Cory, S. and J.M. Adams, *The Bcl2 family: regulators of the cellular life-or-death switch.* Nature Reviews Cancer, 2002. **2**(9): p. 647-656.

58. Kim, W.H., et al., *Synergistic activation of JNK/SAPK induced by TNF-α and IFN-γ: apoptosis of pancreatic β-cells via the p53 and ROS pathway.* Cellular signalling, 2005. **17**(12): p. 1516-1532.

59. Olivier, M., M. Hollstein, and P. Hainaut, *TP53 mutations in human cancers: origins, consequences, and clinical use.* Cold Spring Harbor perspectives in biology, 2010. **2**(1): p. a001008.

60. Galgano, M.T., et al., *Using biomarkers as objective standards in the diagnosis of cervical biopsies.* The American journal of surgical pathology, 2010. **34**(8): p. 1077.

61. Zhao, L., et al., *A nanosystem of copper (II)-disulfiram for cancer treatment with high efficacy and few side effects.* Frontiers of Materials Science, 2021. **15**(4): p. 553-566.

62. Launay-Vacher, V. *Epidemiology of chronic kidney disease in cancer patients: lessons from the IRMA study group*. in *Seminars in nephrology*. 2010. Elsevier.

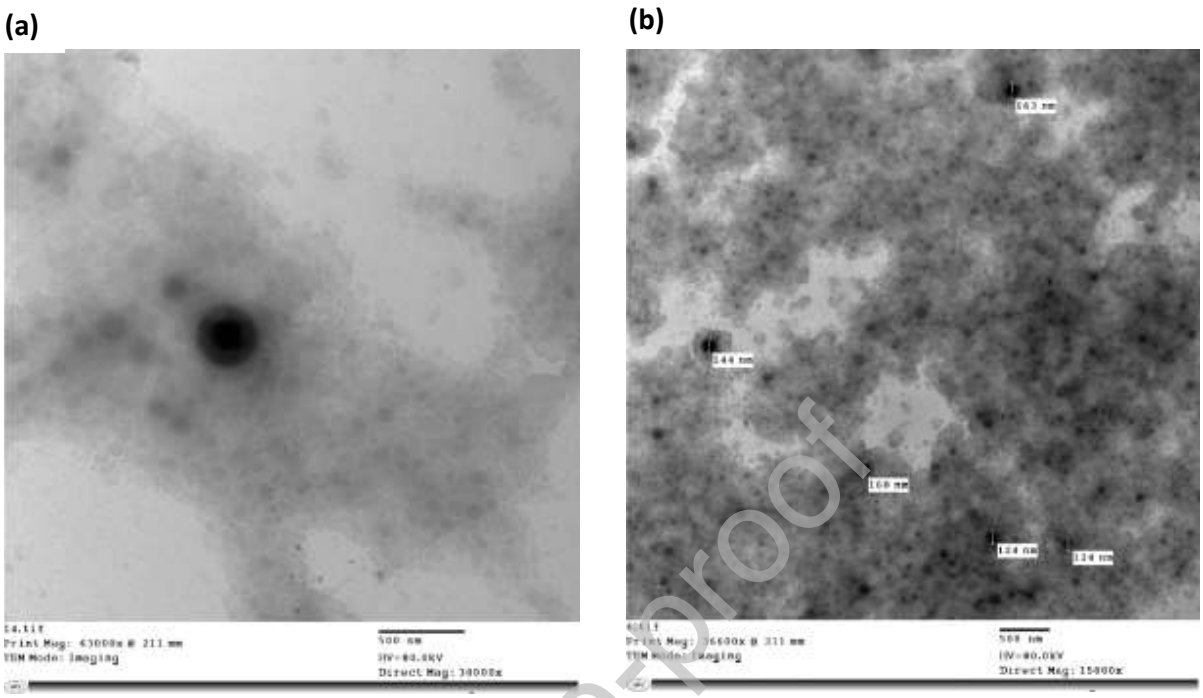

Fig. 1. Transmission electron microscopy (TEM) micrographs of GEM-HNPs at different magnifications: (a) magnification of 30000x and (b) magnification of 15000x.

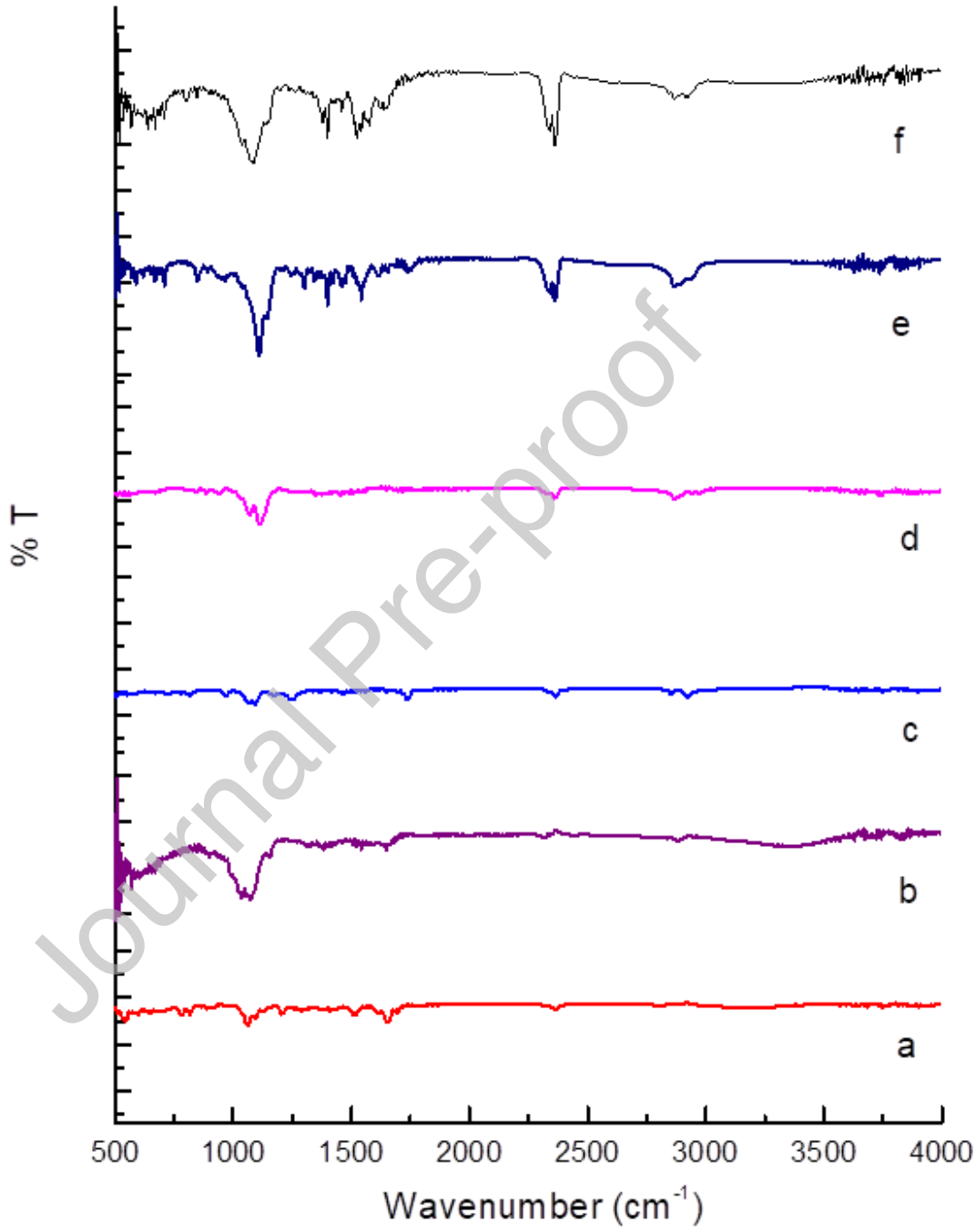

Fig. 2. FTIR spectra of (a) pure gemcitabine powder, (b) chitosan powder, (c) soy lecitin, (d) transcutol (e) physical mixture (f) GEM-HNPs.

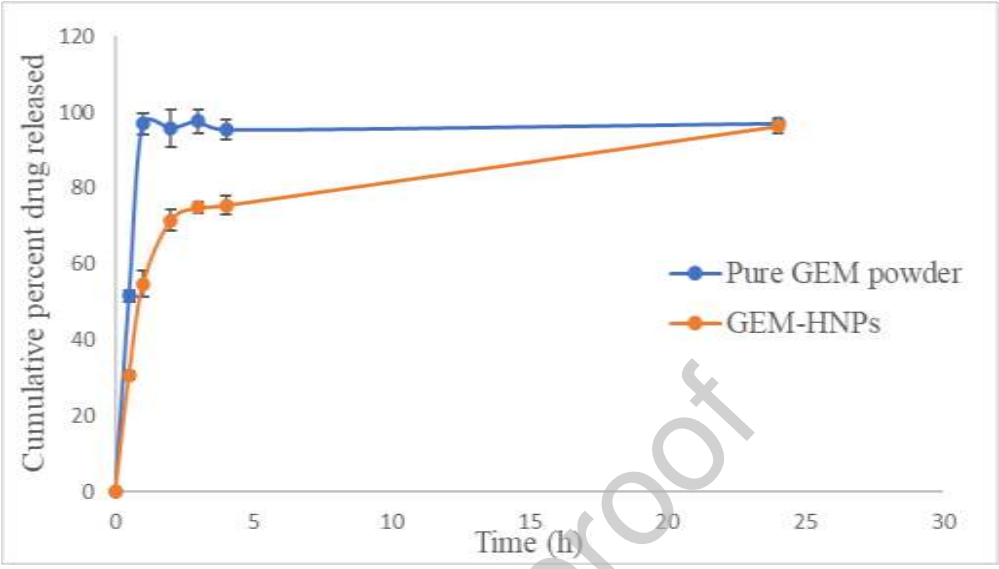

Fig. 3. Comparative release profiles of GEM as its free form and from the selected formulation (F-8) using the dialysis bag diffusion technique in 50 mL acetate buffer (pH 4.5, mimicking vaginal pH) at 37 ± 0.5 °C for 24 h at 50 rpm and temperature 37˚C. Data are mean ± SD (n=3).

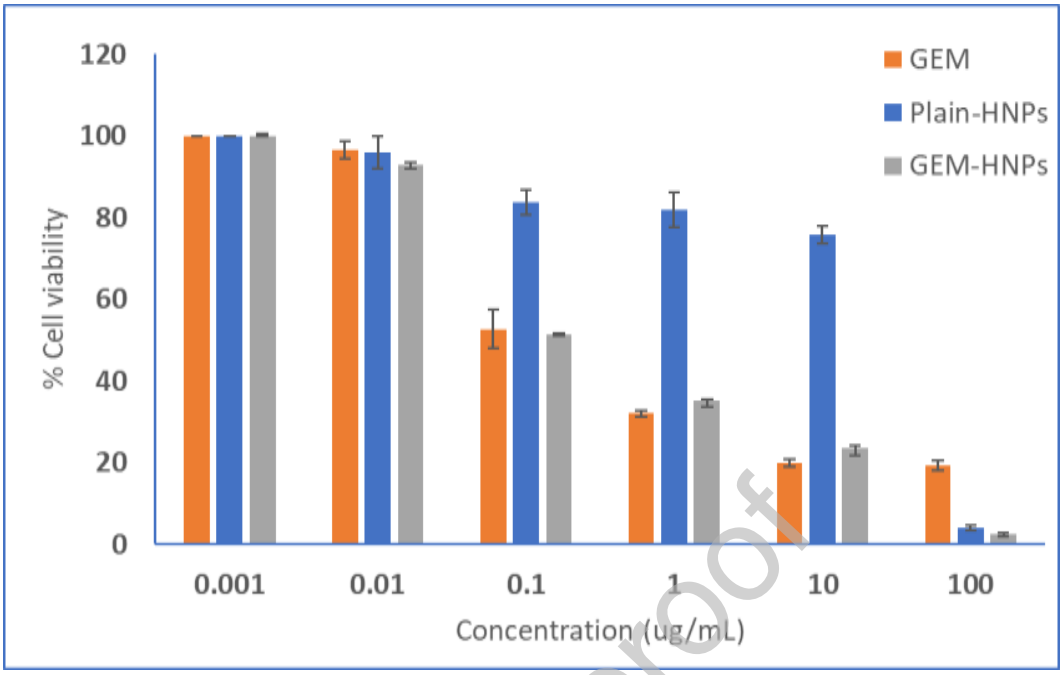

Fig. 4. Cytotoxicity results of pure GEM, plain HNPs and GEM-HNPs (F8) against Hela cancer cell lines after 48h incubation using SRB assay.

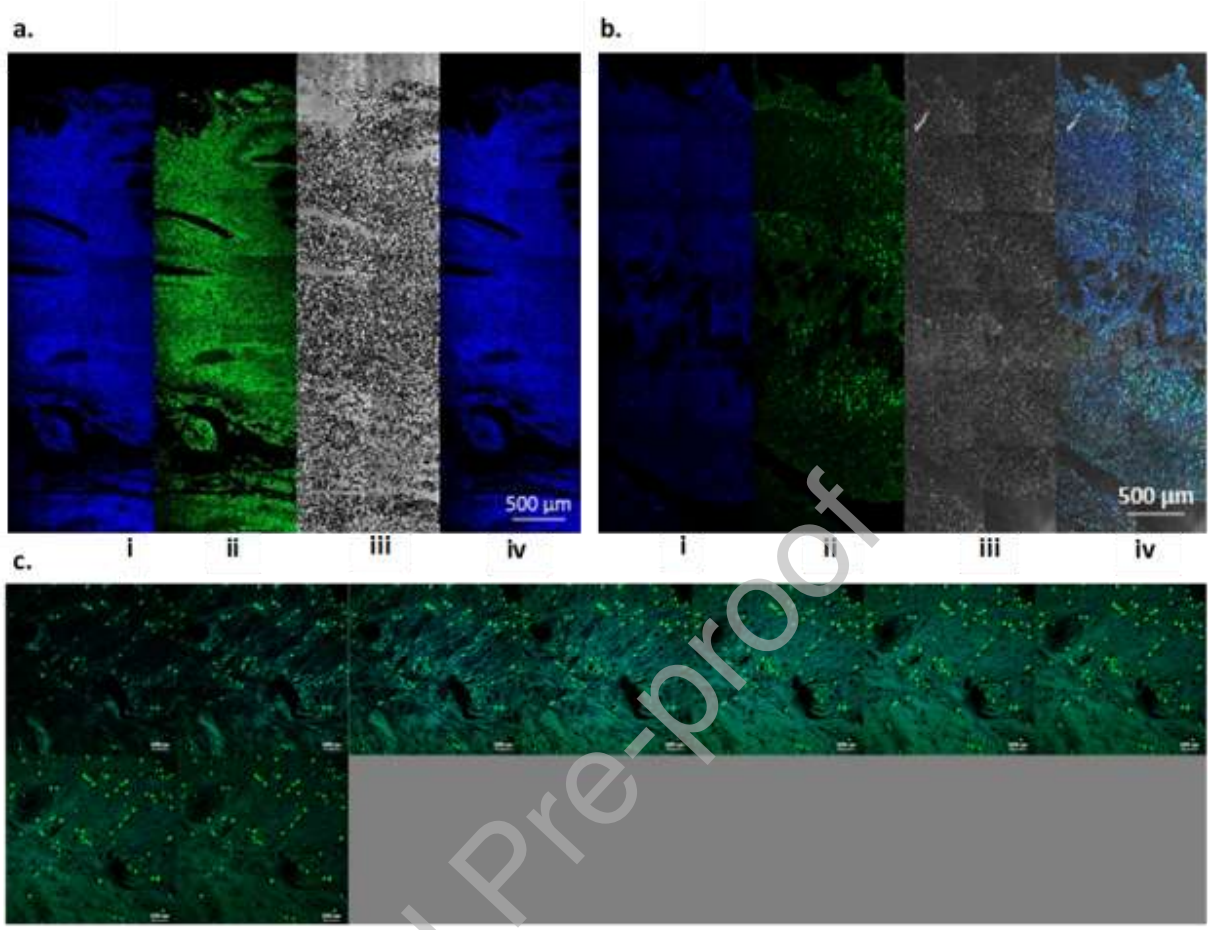

Fig. 5. Confocal images of cervical tissue after intravaginal administration of (a) FITC solution and (b) FITC labeled HNPs: i. blue filter, ii. green filter, iii. no filter, iv. merged filters. Scale bar 500µm (c) Z-stacked images of FITC labeled HNPs. Green channel for FITC: excitation at 543 nm and blue channel for DAPI: excitation at 405nm.Stacked images (Optical slice sections of approximately 2µm) were analyzed using ZEN 2.3 software (blue edition). Scale bar 200µm.

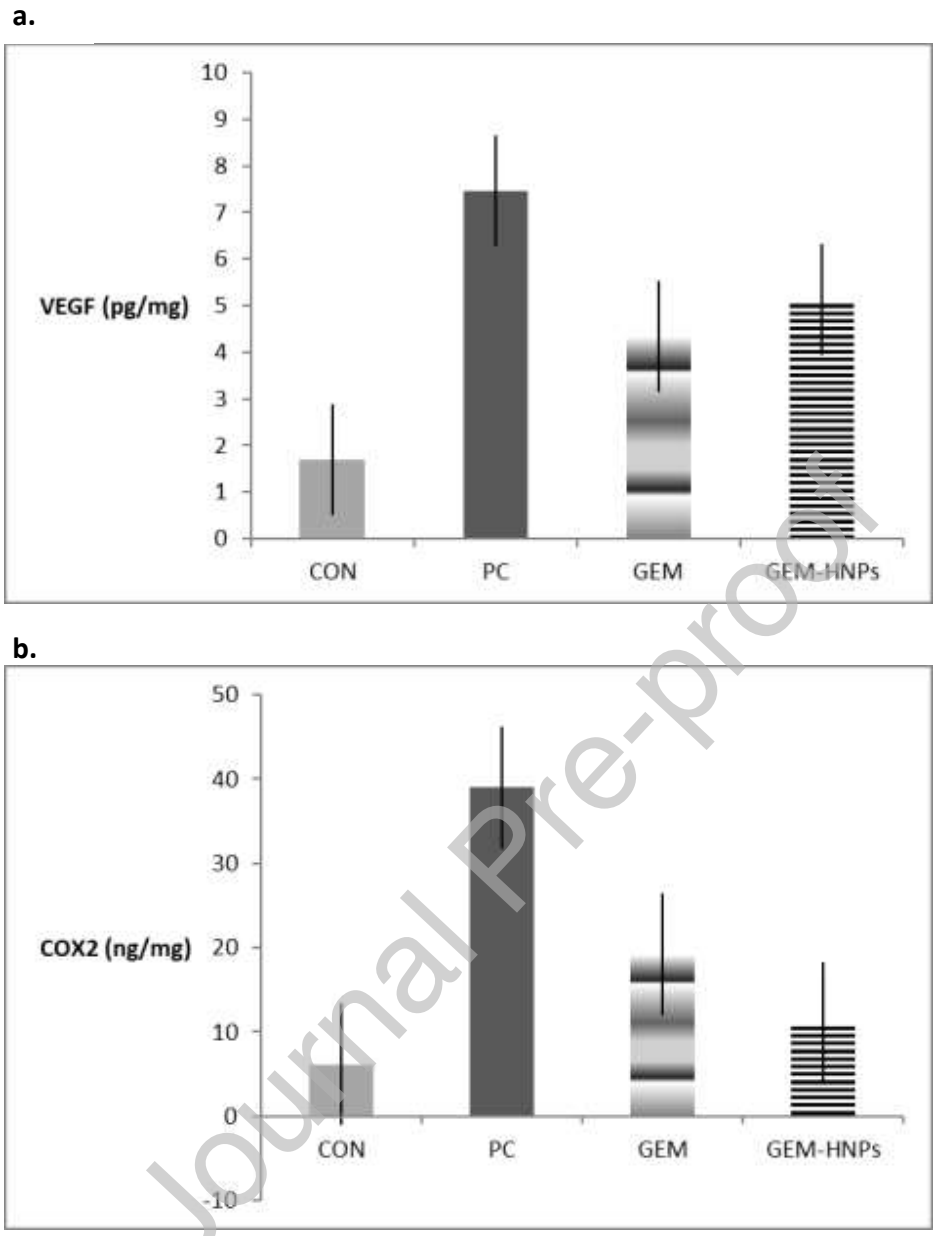

Fig. 6. Relative expression of (a)VEGF, (b) COX-2 in cervical tissues between groups measured using ELISA. Values represent the mean ± SD (P<0.05). CON; Normal control. PC; positive control. GEM; gemcitabine IV. HNPs; gemcitabine loaded hybrid nanoparticles. COX-2, cyclooxygenase-2; VEGF, vascular endothelial growth factor.

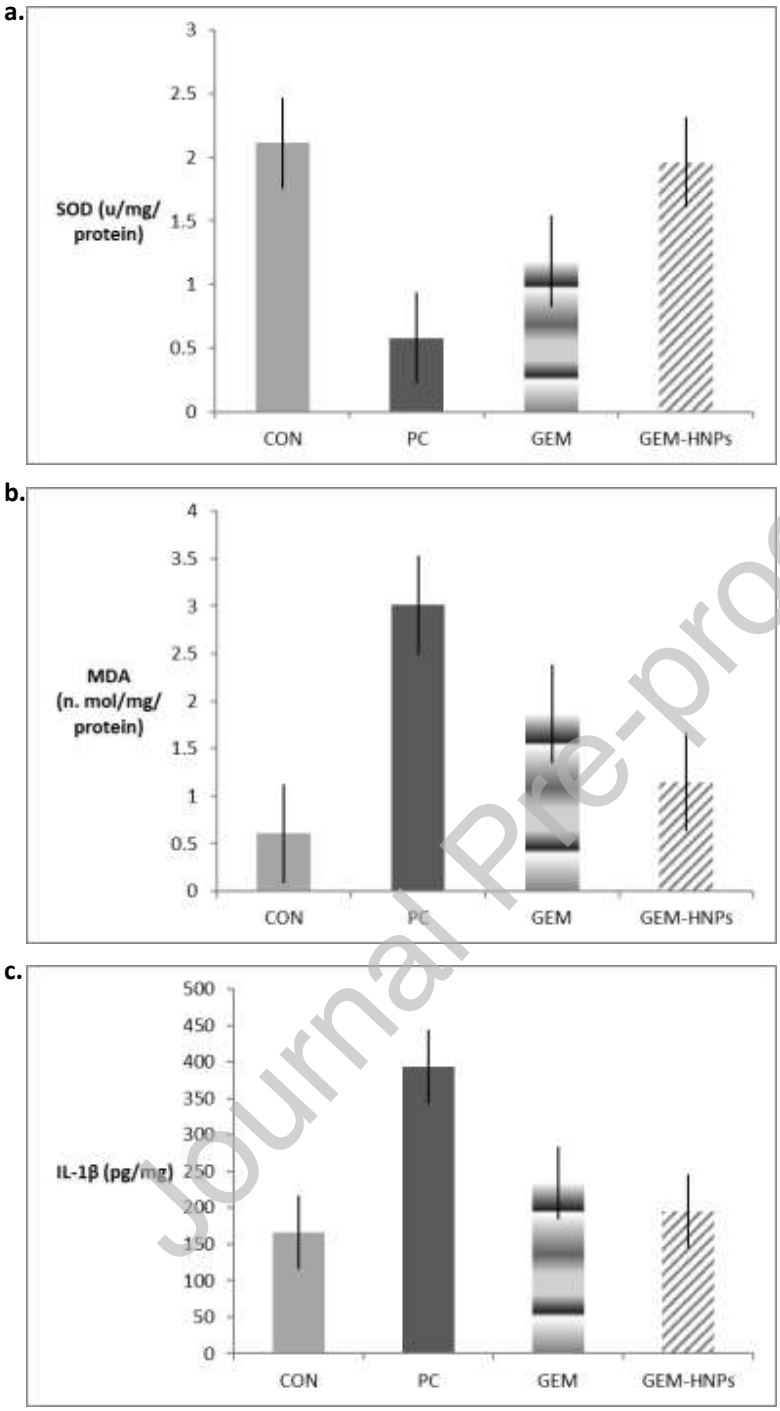

Fig. 7. Cervical level of a) SOD b) MDA c) IL-1B, in all groups. Values represent the mean ± SD ($P<0.05$). CON; negative control. PC; positive control. GEM; gemcitabine IV. HNPs; GEM-HNPs. SOD; superoxide dismutase. MDA; malondialdehyde. IL-1β; interleukin-1β.

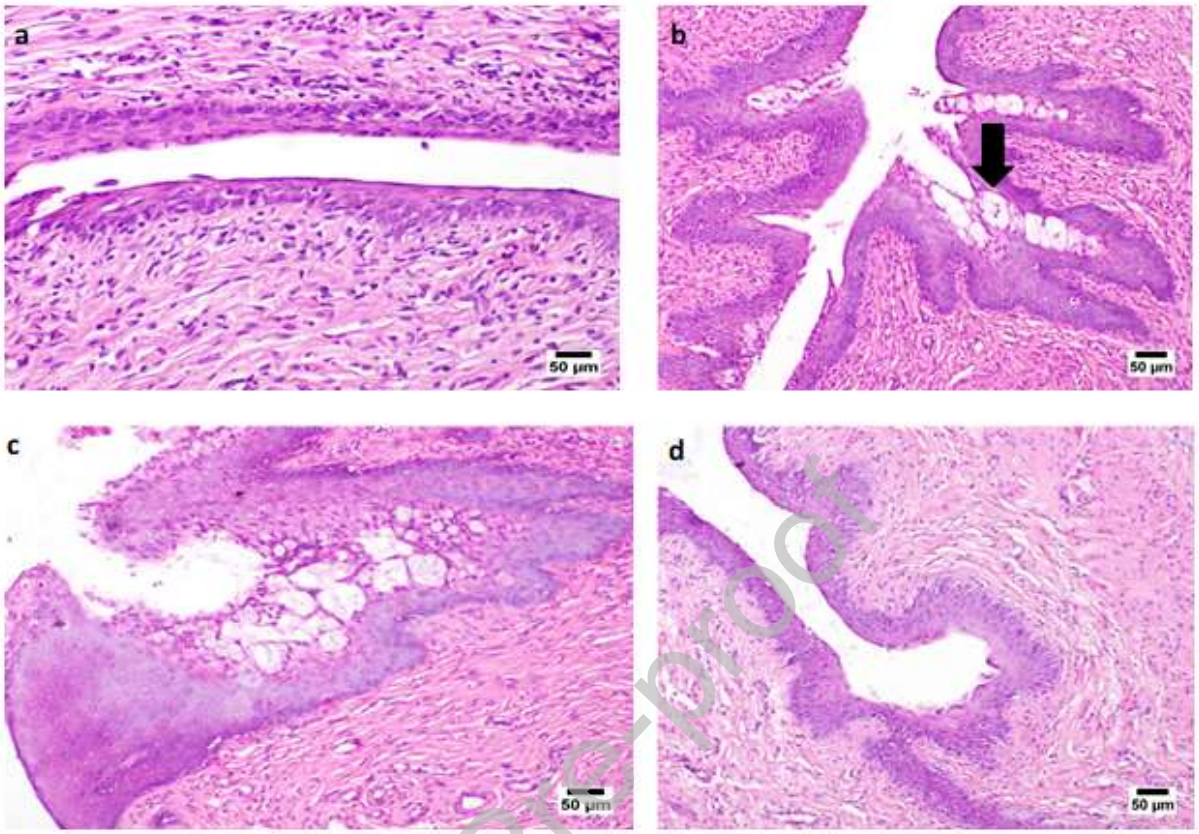

Fig. 8. Histopathology of cervix showing (a) Normal histological structure of mucosa and submucosa in negative control group; (b) Hyperplasic stratified mucosal layer with vacuolation (arrow) in positive control group; (c) Vacuolation in the epithelial cells with dysplasia of mucosal layer in gemcitabine IV group; (d) Mild hyperplastic mucosal surface in GEM-HNPs group (H and E, ×50).

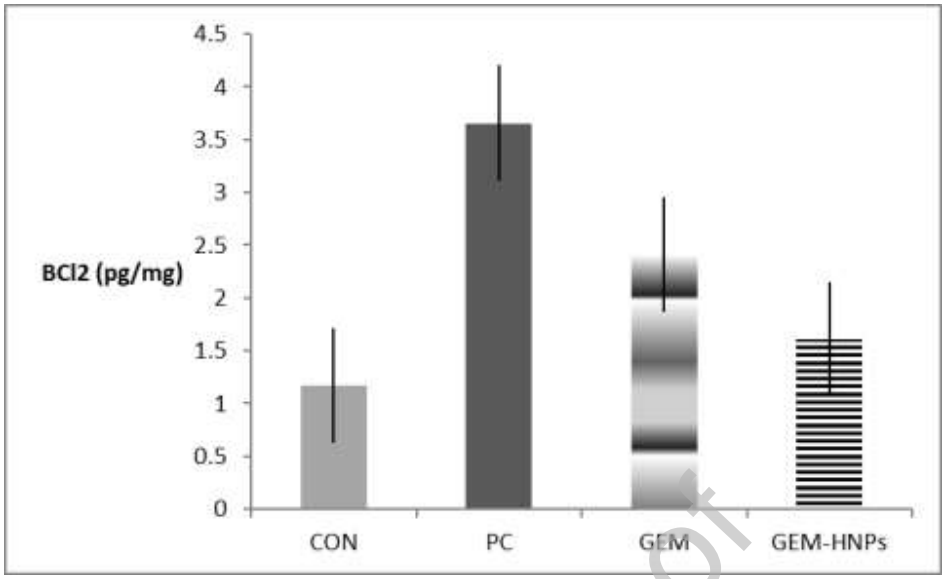

Fig. 9. Protein expression levels of Bcl-2 gene in cervical tissues determined by ELISA. Values represent the mean ± SD ($P<0.05$). CON; Normal control. PC; positive control. GEM; gemcitabine IV. HNPs; gemcitabine loaded hybrid nanoparticles.

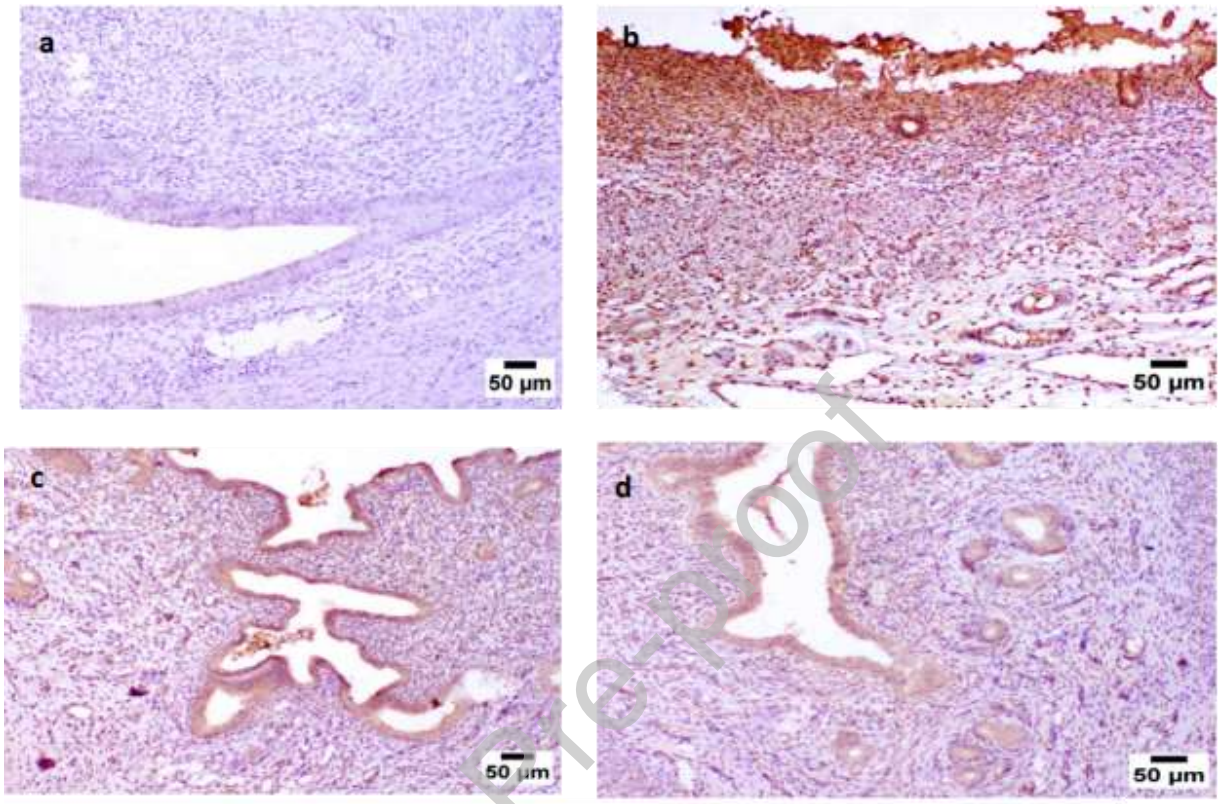

Fig. 10. P53 Expression analysis by Immunohistochemical Staining in in cervical tissues showing (a) Normal negative expression of p53 in the mucosa and submucosa of negative control group (b) strong expression of p53 in the mucosa and submucosa in positive control group (c) moderate expression of p53 in gemcitabine IV group (d) lower expression of p53 in GEM-HNPs group.

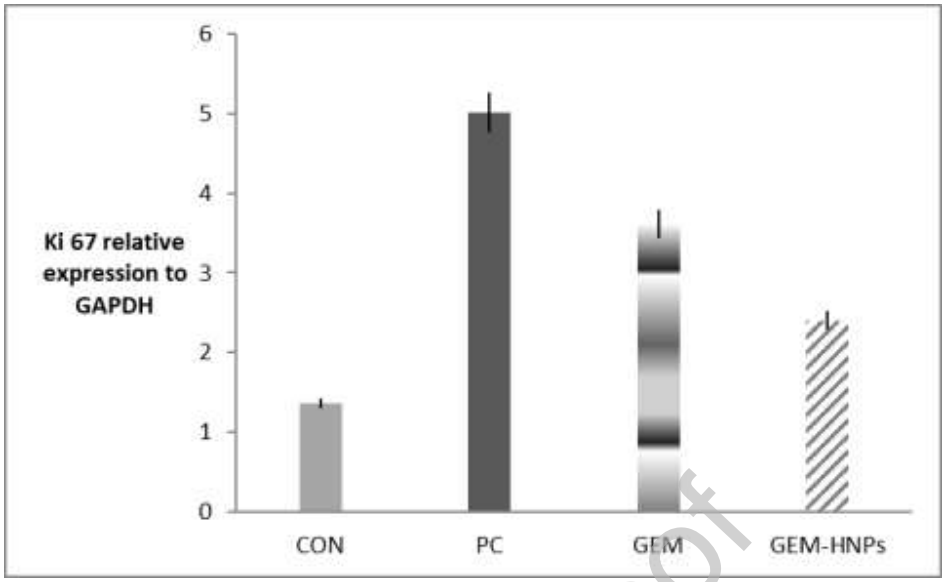

Fig.11. Quantitative RT-PCR analysis of the relative expression of Ki67 gene in the cervices of rats. Values represent the mean ± SD ($P<0.05$). CON; Negative control group. PC; positive control group. GEM; gemcitabine IV. HNPs; gemcitabine hybrid nanoparticles.

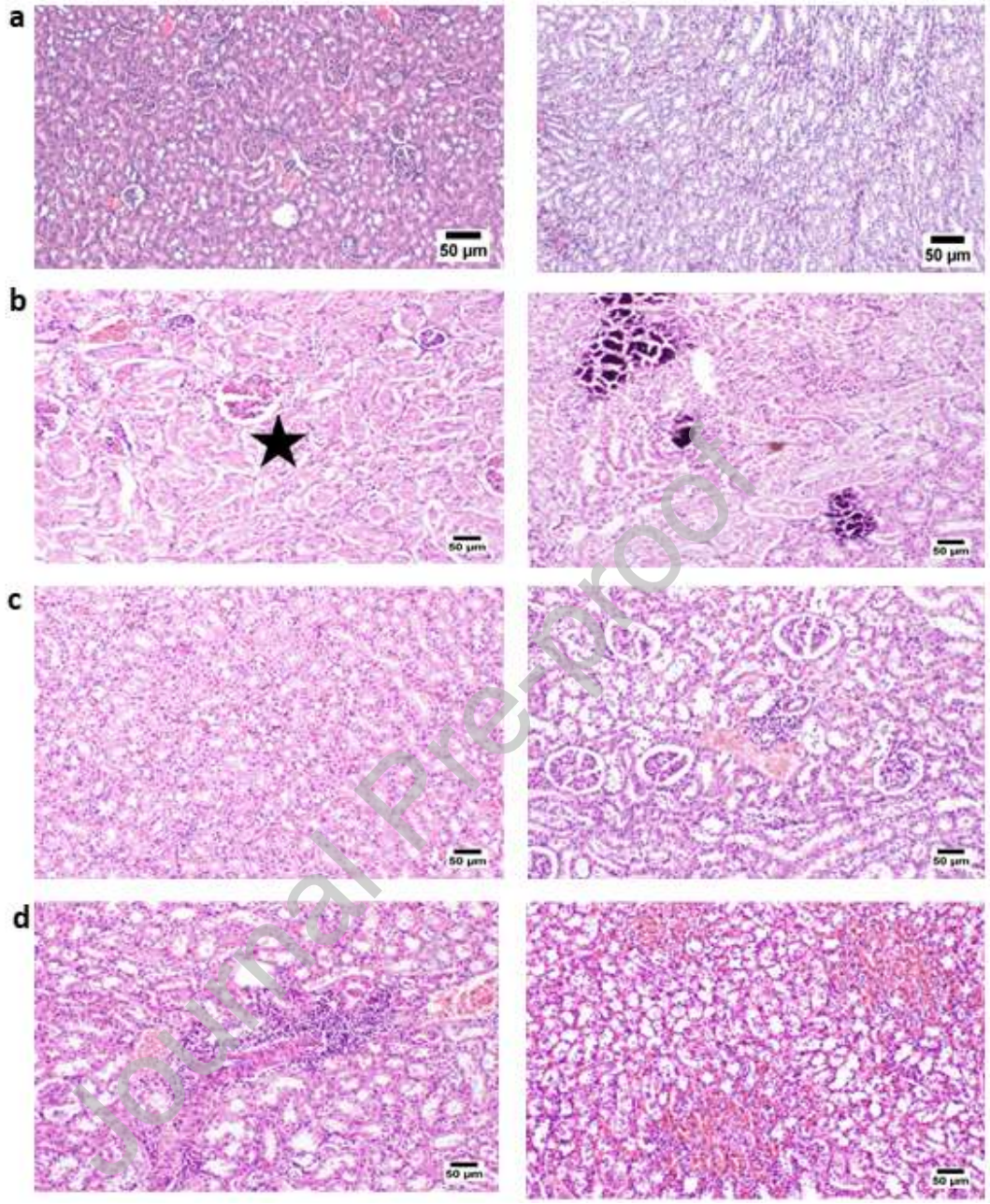

Fig. 12. Histopathology of Kidney showing (a) normal renal cortex in negative control group; (b) severe necrosis of renal tubular epithelium (star) and multifocal mineralized necrotic renal tubules associated with interstitial nephritis in positive control group; (c) necrobiotic changes in the renal tubules with congestion of the peritubular capillaries and degeneration and necrosis of cortical renal tubules with perivascular mononuclear cells infiltration in gemcitabine IV group; (d) mild interstitial nephritis and hyperemic medullary area with necrosis of renal tubules in GEM-HNPs group (H and E, ×50).

Table 1. Formulation variables used in the preparation of GEM-HNPs

Formula	Type of lecithin	Amount of lecithin (mg)	Amount of chitosan (mg)	chitosan/lecithin ratio	Type of surfactant	Amount of surfactant (mg)
F1	Soya	100	20	1:5	-	-
F2	Egg	100	20	1:5	-	-
F3	Egg	150	20	1:7.5	-	-
F4	Egg	100	10	1:10	-	-
F5	Egg	100	30	1:3	-	-
F6	Egg	100	30	1:3	Labrafac	50
F7	Egg	100	30	1:3	Labrasol	50
F8	Egg	100	30	1:3	Transcutol	50
F9	Egg	100	30	1:3	Transcutol	100

Table 2. Characteristics of GEM-HNPs formulations

Formula	PS ± SD (nm)	PDI ± SD	ZP ± SD (mV)	EE % (w/w)	LE % (w/w)
F1	292 ± 8.25	0.372 ± 0.04	14.8 ± 2.05	43 ±2.4	8.6±0.6
F2	174.5 ± 3.6	0.285 ± 0.021	41.7 ± 0.849	55 ± 1.5	11±0.4
F3	163.6 ± 5.58	0.302 ± 0.008	41.4 ± 2.26	52.32 ±4.6	7.8±0.9
F4	155.2 ± 0.424	0.296 ± 0.035	43.3 ± 1.27	56.5 ± 3.6	12.3±1.5
F5	184.6 ± 5.23	0.316 ± 0.061	49.5 ± 0.07	68.5 ±2.1	12.8±0.5
F6	326.7 ± 2.97	0.461 ± 0.002	11.4 ± 0.283	63.25 ±5.5	9.0±1.1
F7	210.4 ± 4.172	0.324 ± 0.074	44.9 ± 0.849	37 ±4.6	5.2±0.9
F8	235.9 ± 11.24	0.290 ± 0.004	43.8 ± 0.495	76.8 ±1.3	10.9±0.2
F9	195.0 ± 2.97	0.373 ± 0.004	47.4 ± 0.424	54.7 ±2.5	6.3±0.4

Credit Author Statement

Mona Elhabak: Conceptualization, Methodology, Software, Writing, Reviewing and Editing.

Samar Ibrahim: Methodology and writing.

Reem R. Ibrahim: Methodology, Software, Writing, Reviewing and Editing.

Declaration of interests

☒The authors declare that they have no known competing financial interests or personal relationships that could have appeared to influence the work reported in this paper.

☐The authors declare the following financial interests/personal relationships which may be considered as potential competing interests:

Author Agreement Statement

We the undersigned declare that this manuscript is original, has not been published before and is not currently being considered for publication elsewhere.

We confirm that the manuscript has been read and approved by all named authors and that there are no other persons who satisfied the criteria for authorship but are not listed.

We further confirm that the order of authors listed in the manuscript has been approved by all of us. We understand that the Corresponding Author is the sole contact for the Editorial process. He/she is responsible for communicating with the other authors about progress, submissions of revisions and final approval of proofs

Signed by all authors as follows:

Mona Elhabak

Samar Ibrahim

Reem Ragaey